Int. J. Heat Mass Transfer. Vol. 12, pp. 1403–1419. Pergamon Press 1969. Printed in Great Britain

ON INCIPIENT-BOILING WALL SUPERHEATS IN LIQUID METALS†

O. E. DWYER

Department of Applied Science, Brookhaven National Laboratory, Upton, New York 11973

(*Received* 14 *November* 1968 *and in revised form* 28 *March* 1969)

Abstract—It is shown that good agreement between predicted and measured incipient-boiling wall superheats can be obtained with Holtz's [4] original superheat model, if two additional factors are taken into consideration. The first of these is the loss of inert gas from the cavity between the time of maximum boiling suppression (MBS) and the time of the incipient boiling (IB) event. The second of these is the probability that the radius of curvature of the liquid-vapor interface at IB may be significantly different from that at MBS.

Based upon the recent experimental IB results obtained by Chen [5] on potassium and those obtained by Holtz and Singer [8] on sodium, the following tentative conclusions have been drawn: (a) The loss of inert gas from an active cavity between the time of MBS and that of the first IB event appears to be negligibly small, but it can be considerable if a large number of IB events follow a single MBS treatment; (b) Bubble radius at IB is about $\frac{2}{3}$ that at MBS; (c) Surface finish for standard smooth surfaces would not appear to have a strong influence on IB superheats; (d) The apparent heat-flux effect could possibly be in reality an inert-gas effect.

NOMENCLATURE

G_0, quantity defined by term in equation (12). It is proportional to the inert gas content of an active cavity at the time of initial filling of the system [(in. lbf)/°R];

h, length of conical vapor space in idealized cavity [in.];

IB, incipient boiling;

n, number of lb-mols of inert gas in cavity at time of nucleation;

MBS, maximum boiling suppression;

p_g^0, partial pressure of inert gas in cavity at time of original filling of the system with liquid metal [psia];

p_G, partial pressure of inert gas in cavity at time of nucleation [psia];

p_L, system (or liquid) pressure at time of nucleation [psia];

p_v, vapor pressure of liquid at time of nucleation [psia];

r, radius of curvature of liquid–vapor interface in cavity at time of nucleation [in.];

r_c, cavity radius at liquid–vapor interface at time of nucleation [in.];

r_0, cavity radius at liquid–vapor interface at time of original filling [in];

R, gas constant [(in. lbf)/(lb mol °R)];

$t_L(\approx t_w)$, temperature of bubble (and cavity) at time of nucleation [°F];

t_L^*, same as t_{sat}[°F];

T_L, same as t_L except on absolute scale [°R];

T_0, temperature of cavity and adjacent liquid at time of original filling [°R];

t_{sat}, saturation temperature corresponding to p_L[°F];

$t_w(\approx t_L)$, temperature of heating surface at time of nucleation, [°F];

V, volume of vapor phase in cavity at time of nucleation [in^3].

† This work was performed under the auspices of the U.S. Atomic Energy Commission.

Greek symbols

α, contact angle measured from vapor side (see Fig. 2) [deg]

β, quantity defined by equation (11). It is characteristic of a given system and proportional to the inert gas content of an active cavity at time of nucleation [(in.)(lb)/°R];

γ, apex angle of conical cavity (see Fig. 2) [deg]

σ, surface tension at $t_L(\approx t_w)$ [lbf/in.].

Superscript

(') represents the value of the particular quantity at the time of maximum boiling suppression (MBS).

INTRODUCTION

WHEN a liquid boils on a heated surface the temperature of that surface is always greater than the bulk temperature of the boiling liquid. we can see *that* from the simple force-balance bubble-equilibrium equation

$$p_v = p_L + \frac{2\sigma}{r}. \tag{1}$$

Thus, in order for a bubble to exist in the liquid, p_v must be greater than p_L. The equation is based on the assumption of a spherical bubble and the absence of inert gas therein. The pressure p_v represents the vapor pressure corresponding to the temperature of the adjacent liquid $t_L(\approx t_w$, for liquid metals); and p_L represents the liquid pressure, for which $t_L^*(=t_{sat})$ is the corresponding saturation temperature. The temperature driving force, $(t_L - t_L^*)$, is known as the superheat requirement; and since nucleation generally occurs on a heating surface, we use the term wall superheat and the symbols $(t_w - t_{sat})$. The superheat given by equation (1) is the minimum value to produce bubble growth, and therefore boiling inception.

Since liquid sodium is used to cool the cores and blankets of fast-breeder, nuclear-power reactors, there is considerable interest in being able to predict incipient-boiling wall superheats, if and when malfunctioning occurs and the system overheats. Incipient-boiling superheats of hundreds of Fahrenheit degrees have been observed [1–3] with alkali metals. It is thus conceivable that large and sudden vapor generation rates could occur, which in turn could increase nuclear reactivity to the point of meltdown of reactor fuel.

Alkali metals, owing to their chemical reduction power, generally wet their containers very well. They also wet the larger cavities (in normal heating surfaces) and render them inactive. This tends to make the incipient-boiling superheats for alkali metals higher than those for ordinary liquids. There are two other reasons why liquid metals tend to give higher incipient-boiling wall superheats than those of ordinary liquids: (a) they have less steep vapor pressure curves in practical temperature ranges, and (b) their capacity to dissolve inert gases increases, rather than decreases, with increase in temperature. The latter characteristic causes liquid metals to absorb inert gases from potential nucleating cavities.

The phenomenon of nucleate boiling initiation in alkali metals is a very complicated one, and the required superheat in a given situation depends upon a large number of variables [4, 5].

As mentioned above, alkali metals tend to quench (and therefore deactivate) the larger cavities and to penetrate (or suppress bubble generation in) the smaller ones; and it is now generally accepted that the wall superheat required to initiate nucleate boiling, in a given situation, depends on the extent to which the metal has penetrated the smaller cavities. It is thus apparent that in the case of alkali metals, bubble growth during boiling incipience occurs most probably *inside* a nucleating cavity. The problem then is to determine the effective value of r for use in equation (1), in order to predict p_v, and from it, t_w. Holtz [4] has proposed a clever way of doing this; and the ideas presented in this paper represent an extension of his.

THEORETICAL CONSIDERATIONS

Let us consider the sodium/stainless-steel system. Before the steel is exposed to sodium, it has an oxide coating. The sodium soon removes the oxide from the superficial surface of the steel, but not from the cavities. However, as time passes, the sodium begins to penetrate the cavities, removing the oxide from their surfaces as it advances. The rate and extent of penetration will depend primarily upon the temperature, the pressure, and the amount of inert gas in the cavity. Such a cavity, based upon Holtz's [4] postulate, is shown schematically in Fig. 1. While the sodium advances into the

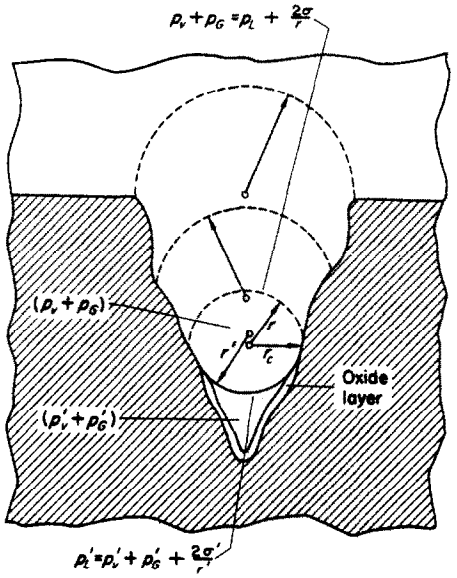

FIG. 1. Illustration of a cavity which is unquenched under subcooled conditions and is capable of becoming active when the temperature is increased. The equations represent the force balances at thermal and mechanical equilibrium. See text for further description.

cavity, it is unwetted at the liquid–vapor interface, because of the presence of the oxide layer.

A force balance at the vapor–liquid interface gives the relation

$$p_v + p_G + \frac{2\sigma}{r} = p_L. \tag{2}$$

The partial pressure of the inert gas, p_G, may vary a good deal, depending on the pressure at which the system was filled with sodium. For a freshly charged system, p_G can be either much smaller than, comparable to, or much greater than p_v; while for a circulating system which has been operating for some time, as, for example, the fuel element surface in a sodium-cooled reactor, p_G could be relatively small. For a nonwetting situation, the presence of the inert gas is, of course, not required to maintain the liquid–vapor interface. At the point of farthest penetration, we can rewrite equation (2) in the form

$$p_L' - p_v' - p_G' = \frac{2\sigma'}{r'}, \tag{2a}$$

where the primes on the symbols represent the conditions that then exist, which, in turn, constitute the state of maximum boiling suppression (MBS).

Holtz [4] assumed that p_G' was negligibly small and recommended that r' as calculated from the above equation be used in equation (1) to calculate p_v. This gives the equation

$$\frac{p_v - p_L}{p_L' - p_v'} = \frac{\sigma}{\sigma'} \tag{3}$$

from which p_v can be solved directly, when the temperature and pressure at MBS, and the system pressure at incipient boiling are known. The superheat is then readily obtained from vapor pressure information. Later, Chen [5] included p_G' in equation (2a) and, in effect, assumed a value for the amount of inert gas trapped in the cavity, which enabled him to calculate superheats which gave reasonable agreement with forced-convection incipient-boiling superheat measurements in potassium. Chen's method of predicting incipient-boiling wall superheats is discussed briefly later on. In the present paper, the author shows that the amount of inert gas in an active cavity does not remain constant and that r and r' are most probably not equal. With these changes, it is possible to get excellent agreement between predicted and measured superheats.

Cavities may have different shapes, but they are generally considered to be more conical than cylindrical. For the sake of discussion, let us assume that our reference cavity is a right cone. This is shown schematically in Fig. 2.

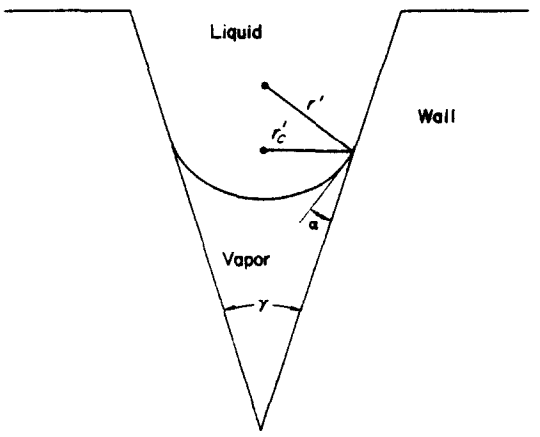

FIG. 2. Idealized representation of the cavity shown in Fig. 1 when the liquid–vapor interface is in its maximum-boiling-suppression state. The pertinent geometrical parameters are illustrated.

for the subcooled, MBS condition. We can relate r' to the cavity radius, r'_c, at farthest penetration, by the equation

$$r' = \frac{r'_c}{\cos\left[(\gamma/2) + \alpha\right]} \tag{4}$$

where γ is the apex angle and α is the contact angle measured from the *vapor* side, as illustrated in the figure. The above equation represents, of course, the so-called "nonwetting" case, in which $0° \leqslant \alpha \leqslant 90°$.

If we assume the perfect-gas law, which is quite valid in this case, we can write

$$p'_G = \frac{n'RT'_L}{V'} \tag{5}$$

where n', T'_L, and V' represent the number of moles of inert gas in the cavity, the absolute temperature of the cavity, and the volume of the cavity, at the time of farthest penetration of liquid into it.

If we assume the cavity to be long and narrow, which it most likely is, in alkali-metal systems, we can neglect the curvature of the liquid–vapor interface and simply express the gaseous volume of the cavity as

$$V' = \tfrac{1}{3}\pi(r'_c)^2 h', \tag{6}$$

where

$$h' = r'_c/\tan(\gamma/2).$$

Substituting equations (5) and (6) into (4), and then (4) into (2a), gives

$$p'_L - p'_v - \frac{\beta' T'_L}{(r')^3} = \frac{2\sigma'}{r'} \tag{7}$$

where

$$\beta' = \frac{3n'R\left(\tan\dfrac{\gamma}{2}\right)}{\pi\left[\cos\left(\dfrac{\gamma}{2}+\alpha\right)\right]^3} \tag{8}$$

and may be considered a characteristic quantity, for a given surface-liquid system and a given set of boiling-suppression conditions. Thus, in calculating r' by means of equation (7), β' can be either treated as a parameter or estimated in advance from experimental measurements.

Let us look at Fig. 2 again. If, at some point in time, heating occurs, then, because of an increase in p_v, the interface will begin to recede while still concave on its liquid side. It does not recede a significant distance before it experiences a highly wetted surface, flips over, and becomes convex on its liquid side. When this happens, we can write the force-balance equilibrium equation

$$p_v + p_G - p_L = \frac{2\sigma}{r}. \tag{9}$$

In a similar manner as before, we can write

$$p_G = \frac{nRT_L}{V}, \text{ and} \tag{5a}$$

$$V = \pi r_c^2 h. \tag{6a}$$

where,

$$h = r_c/\tan\left(\frac{\gamma}{2}\right).$$

However, it is logical to assume that $r_c = r'_c$, because that is the cavity radius at which the spherical interface is the most stable (i.e. requires the most superheat for bubble growth), and therefore the one at which nucleation occurs. Thus, remembering this, and proceeding as before, we can convert equation (9) to

$$p_v + \frac{\beta T_L}{(r')^3} - p_L = \frac{2\sigma}{r} \tag{10}$$

where

$$\beta = \frac{3nR\left(\tan\frac{\gamma}{2}\right)}{\pi\left[\cos\left(\frac{\gamma}{2}+\alpha\right)\right]^3} \tag{11}$$

The largest superheat required for bubble growth exists when $r = r_c$; so that when heating causes r to increase above this critical value, the liquid–vapor interface becomes unstable and a bubble of vapor shoots out of the cavity.

The only difference in the expressions for β and β' is the number of moles of inert gas present in the cavity. Thus, the ratio β/β' equals n/n' and represents the fraction of the original inert gas remaining in the cavity at the time of bubble nucleation.

Equations (7) and (10) can be used to calculate incipient-boiling wall-superheat curves when β', β/β', and r/r' are known or treated as parameters. It is obviously impossible to measure these quantities directly; but, if experimental data are taken over sufficient ranges of the prime independent variables, the data can be matched with the curves to yield a unique set of values of β', β/β', and r/r' for a given set of operating conditions.

The ratio β/β' can generally be expected to vary over the range from 0 to 1; but, conceivably, it can also exceed 1, under certain circumstances. If incipient boiling occurs immediately after the suppression condition, β/β' can approach unity, particularly if the heat flux and t_{sat} are relatively low. If, however, incipient boiling occurs after a series of prior incipient boilings following a single suppression, then β/β' can approach zero, particularly if the heat flux and t_{sat} are both relatively high.

The ratio r/r', on the other hand, should not vary so widely. For a cavity approaching the shape of a right cylinder, and for complete nonwetting during boiling suppression and complete wetting at boiling inception, the ratio should approach unity. It is difficult to see how r/r' could be greater than one, because, if anything, there is most probably better wetting during the nucleation stage than nonwetting during the suppression stage, which would tend to make $r < r'$. In the case of conical cavities, even with completely nonwetting liquid–vapor interface during MBS and a completely wetting liquid–vapor interface at IB, the ratio r/r' must be always <1. In the present study, it was found to be around 0·70–0·75 for a set of experimental results on potassium.

Chen's method

Chen [5] also extended Holtz's [4] model and solved equations (2a) and (9) by assuming an idealized conical cavity. In his analysis, he assumed that α equalled 0°, and left p'_G to be empirically evaluated from superheat data. On this basis, his final equation for evaluating r'_c was

$$(r'_c)^3 - \frac{2\sigma' \cos(\gamma/2)}{p'_L - p'_v}(r'_c)^2 - \frac{G_0 T'_L}{(p'_L - p'_v)F(\gamma)} \tag{12}$$

where

$$F(\gamma) = 1 - \frac{\left(\tan\frac{\gamma}{2}\right)\left(1-\sin\frac{\gamma}{2}\right)^2\left(2+\sin\frac{\gamma}{2}\right)}{\left(\cos\frac{\gamma}{2}\right)^3}$$

and where

$$G_0 = \frac{p^0_g r^3_0}{T_0}$$

or a measure of the number of moles of inert gas in the cavity at the time the system was filled with the liquid metal.

Chen recognized that inert gas could diffuse out of the cavity; but, in the derivation of his equation, he assumed the diffusion rate negligible. On that basis, and knowing $r_c'(=r_c=r)$, he derived the equation

$$p_v - p_L = \frac{\sigma(p_L' - p_v')}{\sigma' \cos(\gamma/2)} - \frac{G_0}{(r_c)^3} \times \left[\frac{T_L}{[1 + 2\tan(\gamma/2)]} + \frac{\sigma T_L'}{\sigma' \cos(\gamma/2) \cdot F(\gamma)}\right] \quad (13)$$

for $(p_v - p_L)$, from which the superheat is obtained from vapor pressure information.

In the above equations, there are two empirical quantities—G_0 and γ—because there is no way of directly measuring either. As we shall see later, Chen found the latter to approach zero, in correlating his IB superheat results on potassium, which in effect makes $r = r'$.

CALCULATED RESULTS

Equations (7) and (10) were used to calculate the families of curves in Figs. 3–5. To obtain the curves in Fig. 3, β was taken as a parameter,

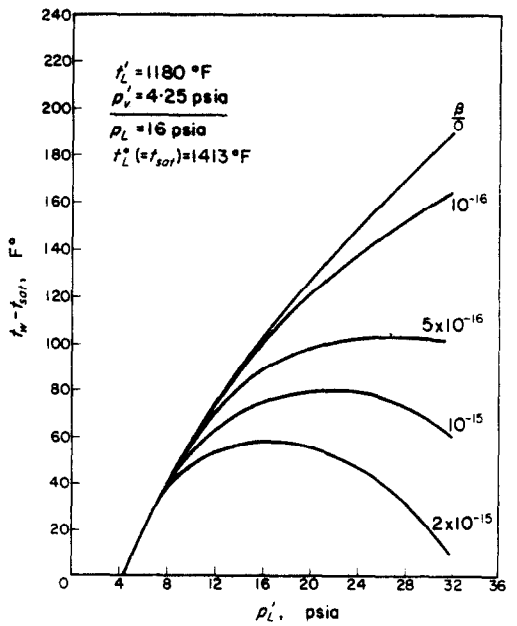

FIG. 3. Incipient-boiling wall superheats for potassium calculated from equations (7) and (10) showing the effects of changes in p_L' and inert gas content. The curves are based on the assumption that $r = r'$.

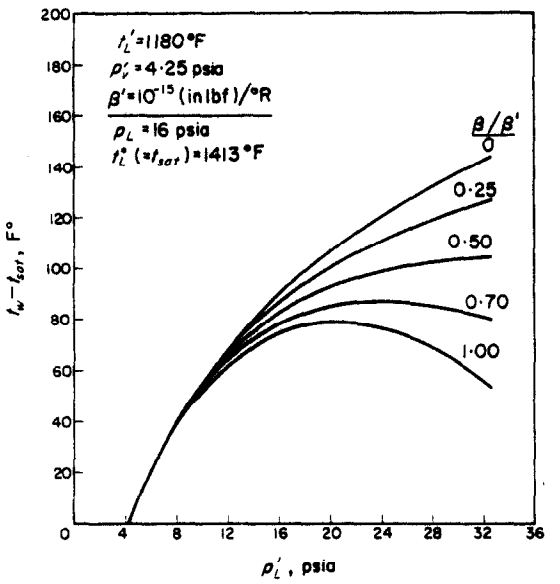

FIG. 4. Incipient-boiling wall superheats for potassium calculated from equations (7) and (10) showing the effects of changes in p_L' and inert gas content. The curves are based on the assumption that $r = r'$.

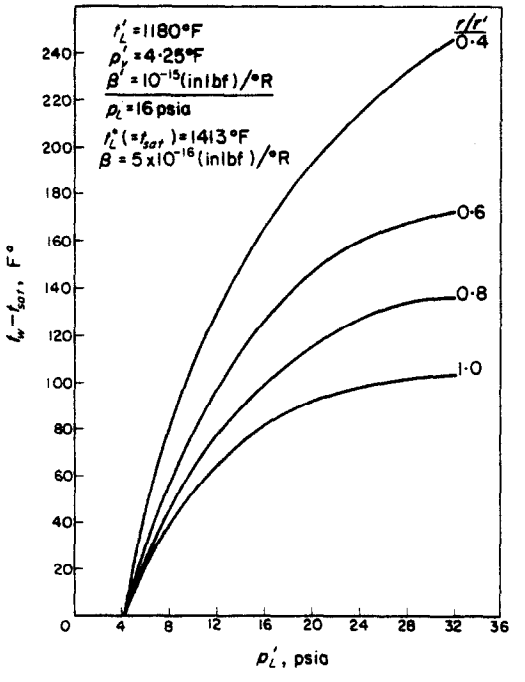

FIG. 5. Incipient-boiling wall superheats for potassium calculated from equations (7) and (10), showing the effects of changes in p_L' and r/r'.

and both the ratios β/β' and r/r' were taken as unity. The condition of $\beta/\beta' = 1$ is approached when each nucleation is preceded by the suppression step. It assumes no inert gas loss from the cavity between those two events, which may not always be true either. However, the condition of $\beta/\beta' = 1$ is a condition that can be approached. The calculation procedure was as follows: The value of r' was calculated from equation (7), after choosing a value of β' and knowing the values of all the other variables in the equation. Then, T_L was calculated from equation (10) by successive approximation, since p_v and σ depend upon T_L. Finally, knowing p_v and p_L, we get t_w and t_{sat} from the vapor pressure curve. In this study, for potassium, vapor pressure and surface tension values were obtained from the equations of Hicks [6] and Cooke [7], respectively.

With reference to Fig. 3, it is instructive to examine Table 1 to see how the respective dependent and independent variables varied, in the calculation of the different curves. As Chen [5] already showed, at low suppression pressures, the incipient-boiling wall superheat is independent of the amount of inert gas trapped in the cavity. On the other hand, as Fig. 3 strikingly shows, the superheat is extremely sensitive to the amount of entrapped gas, at high MBS pressures. The reason for this is that at low values of p'_L, r' is large, and p_G remains small; whereas at high values of p'_L the reverse is true. Still referring to the table, it will be noticed that the values of $r'(=r)$ are typical of those generally estimated from boiling-alkali-metal superheat data.

Returning to Fig. 3 again, we see that at high values of β, the incipient-boiling superheat goes through a maximum as p'_L is varied. This is due to the fact that at high values of p'_L and β, p_G becomes large because r is small; and since p_G is large, p_v does not have to be so great to produce nucleation. The curves in Fig. 3 produce an explanation of why superheat data have sometimes been so "wild" and "unmangeable" in the past, when all the pertinent variables were not carefully controlled and accounted for in the correlations. Even if there were good control and accurate measurement of the various pertinent parameters, we see from the curves that there are certain inert gas contents where $(t_w - t_{sat})$ does not change markedly for moderate changes in p'_L and other inert gas contents where an increase in p'_L produces a decrease in $(t_w - t_{sat})$—the opposite to what one would normally expect.

Figure 4 shows the effect of loss of inert gas from a cavity between the time of maximum boiling suppression and the time of bubble initiation. As in Fig. 3, and for the same reason, we see that at low values of p_L the incipient boiling superheat is unaffected by inert gas loss. The $\beta/\beta' = 0$ curve is lower than the $\beta = 0$ curve in Fig. 3 because the Fig. 4 curve is based upon a larger r' $(=r)$. As in Fig. 3, the curves in Fig. 4 are based on the assumption that $r = r'$.

Figure 5 shows the effect of varying the ratio r/r' for the situation where $\beta' = 10^{-15}$ and $\beta = 5 \times 10^{-16}$, i.e. half of the inert gas escaping from the cavity between the times of maximum boiling suppression and incipient boiling. Unlike the parameters β' and β/β', the parameter r/r' is about equally influential throughout the whole p'_L range, i.e. its relative effect at low values of p'_L is the same as that at high values of p'_L.

From the curves in Figures 3–5, it is possible to choose the correct combination of β', β/β', and r/r' to produce a curve which will correlate a set of experimental results, if they were obtained over a sufficiently wide p'_L range. If the experimental results are sufficiently precise to define a definite curve, there is only one combination of β' vs. p'_L relation, β/β', and r/r' which can satisfy them. There are only two sets of incipient-boiling superheat data reported in the literature where all the prime variables were controlled and their values reported—the potassium results reported by Chen [5] and the sodium results reported by Holtz and Singer [8]. We shall now examine these results and show that equation (7) and (10) can correlate them.

Table 1. Summary of both **MBS** *and* **IB** *conditions pertaining to curves in Fig. 3*

	$\beta' = \beta = 0$			$\beta' = \beta = 10^{-16}$			$\beta' = \beta = 5 \times 10^{-16}$		
p'_L (psia)	8	18	28	8	18	28	8	18	28
p'_v (psia)	4·25	4·25	4·25	4·25	4·25	4·25	4·25	4·25	4·25
p'_G (psia)	0	0	0	0·008	0·35	1·61	0·038	1·38	4·90
t'_L (°F)	1180	1180	1180	1180	1180	1180	1180	1180	1180
$r'(=r)$ (in.)	$2·76 \times 10^{-4}$	$7·53 \times 10^{-5}$	$4·36 \times 10^{-5}$	$2·77 \times 10^{-4}$	$7·75 \times 10^{-5}$	$4·67 \times 10^{-5}$	$2·78 \times 10^{-4}$	$8·40 \times 10^{-5}$	$5·51 \times 10^{-5}$
p_v (psia)	19·45	27·95	35·94	19·25	27·13	32·8	19·30	25·1	26·3
p_G (psia)	0	0	0	0·009	0·43	1·98	0·044	1·65	5·90
p_L (psia)	16·0	16·0	16·0	16·0	16·0	16·0	16·0	16·0	16·0
$t_L (= t_w)$ (°F)	1452	1527	1582	1451	1524	1564	1450	1507	1514
$t^*_L (= t_{sat})$ (°F)	1413	1413	1413	1413	1413	1413	1413	1413	1413
$(t_w - t_{sat})$ (F°)	39	114	169	38	111	151	37	94	101

	$\beta' = \beta = 10^{-15}$			$\beta' = \beta = 2 \times 10^{-15}$		
p'_L (psia)	8	18	28	8	18	28
p'_v (psia)	4·25	4·25	4·25	4·25	4·25	4·25
p'_G (psia)	0·07	2·25	6·98	0·14	3·32	9·16
t'_L (°F)	1180	1180	1180	1180	1180	1180
$r'(=r)$ (in.)	$2·80 \times 10^{-4}$	$9·00 \times 10^{-5}$	$6·17 \times 10^{-5}$	$2·88 \times 10^{-4}$	$9·95 \times 10^{-5}$	$7·10 \times 10^{-5}$
p_v (psia)	19·2	23·4	22·4	19·04	21·27	18·63
p_G (psia)	0·09	2·68	8·28	0·16	3·91	10·45
p_L (psia)	16·0	16·0	16·0	16·0	16·0	16·0
$t_L (= t_w)$ (°F)	1449	1490	1480	1448	1470	1444
$t^*_L (= t_{sat})$ (°F)	1413	1412	1412	1413	1413	1413
$(t_w - t_{sat})$, (F°)	36	78	68	35	57	31

COMPARISON BETWEEN THEORY AND EXPERIMENTAL RESULTS

Potassium

The only available incipient-boiling wall superheat results, where all the important variables were controlled and measured, are those recently reported by Chen [5]. Using a vertical 0·622 in. i.d. cylindrical channel, he determined the independent effects of p'_L, t'_L, and p_L for forced, vertical flow of potassium. The linear velocity through the channel was held constant at 0·2 ft/s, and the heat flux was also held fairly constant at ≈50,000 Btu/(h·ft^2). The test section was made of Haynes 25 alloy, and its inside surface had a smooth gun-drilled surface, with a range of cavity sizes of 10^{-6}–10^{-2} in.

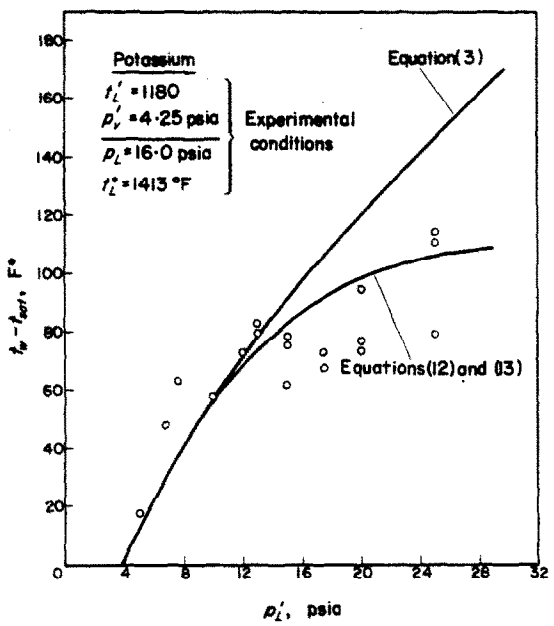

FIG. 6. Incipient-boiling superheat results obtained by Chen [5] compared with Chen's and Holtz's theoretical curves.

Figure 6 presents some data obtained by Chen [5] showing the effect of p'_L on the incipient-boiling wall superheat. Although there is appreciable scatter in the data points, nevertheless they are probably the most precise superheat results yet reported on a liquid metal. Two theoretical curves are also shown—that by equation (3), which was originally proposed by Holtz [4], and that by equations (12) and (13), proposed by Chen [5]. The former is actually the same as the $\beta = 0$ curve in Fig. 3. The latter is a best-fit curve produced by taking γ equal to zero and G^0 equal to 8×10^{-17} (in. lbf)/°R. The great improvement in the Holtz model by allowing for the inert gas content is obvious, but it is also apparent that there is still room for further improvement.

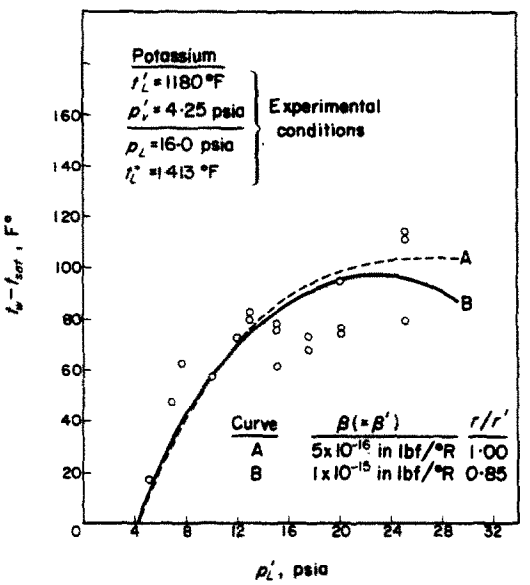

FIG. 7. Comparison between the incipient-boiling superheat results of Chen [5] and two theoretical curves each based upon equations (7) and (10). Values of β and r/r' were chosen to give best fits to the experimental points.

The same data points are shown in Fig. 7 where two other curves are drawn, each obtained from simultaneous solutions of equations (7) and (10). Curve A is based on the assumption of $\beta = \beta' = 5 \times 10^{-16}$ (in. lbf)/°R and $r = r'$. It is the best fitting curve that can be obtained from equations (7) and (10), when loss of inert gas from the cavity is not considered and when

the radius of curvature of the liquid–vapor interface at the time of bubble growth (under wetting conditions) is the same as that at the time of maximum boiling suppression (nonwetting conditions). It is therefore not surprising that curve A is practically identical with the lower curve in Fig. 6.

Curve B in Fig. 7 is the best one that can be obtained from equations (7) and (10), when r/r' is allowed to vary, still keeping β equal to β'.

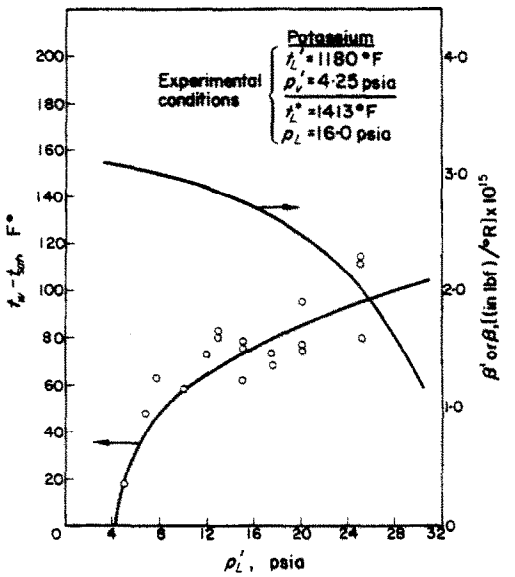

FIG. 8. Correlation of Chen's incipient-boiling superheat results by equations (7) and (10). The ratio r/r' was taken equal to 0·70, and $\beta(=\beta')$ was taken as represented by the second curve shown in the figure.

It is apparent that neither of these curves gives as good a fit to the data points as that in Fig. 8. That curve was obtained by taking one additional variable into consideration, i.e. the ratio of β to β', or the gradual loss of inert gas from the cavity. The data in Fig. 8 were obtained by (a) heating the test section to 850°F, (b) evacuating to 0·3 psia, (c) charging the potassium, (d) maintaining the system at 1180°F and a low pressure (p_L') for two hours and (e) measuring t_w at boiling inception for a system pressure (p_L) of 16 psia. Then a succession of data points was obtained by repeating steps (d) and (e), carrying out step (d) at successively higher pressures. It is thus logical to conclude that, over this period, there was some gradual loss of inert gas from the active cavities. The curve in Fig. 8 was calculated for an original value of β' of $3{\cdot}1 \times 10^{-15}$ (in. lbf)/°R and a gradual reduction of $\beta'(=\beta)$ with time. This reduction is indicated by the β curve in the figure. The increasing negative slope of this curve with increase in p_L' (or time) is very reasonable, because the greater loss of inert gas would naturally occur at the higher wall temperatures.

The curve in Fig. 8 represents a unique solution of equations (7) and (10), where $\beta(=\beta')$, and r/r' are specified. Only an r/r' value of 0·70 and the β curve as shown will produce that curve. Over the time period during which the data points in Fig. 8 were obtained β dropped from $3{\cdot}1 \times 10^{-15}$ to $2{\cdot}0 \times 10^{-15}$, indicating that approximately $\frac{1}{3}$ of the original inert gas content of the cavity had escaped, which is not a high fraction. Consequently, for any single given value of p_L' (at which the MBS condition was imposed) β was assumed to be equal to β'. It is seen that the superheat curve in Fig. 8 is higher at the lower values of p_L' and lower at the higher values of p_L' than the curves in the two previous figures. In calculating the last curve, the first difference is due to the fact that r was not taken equal to r', while the second difference is due to the fact that β' was not assumed constant. Thus, in calculating the superheat curve in Fig. 8 from equations (7) and (10), only two independent variables had to be arbitrarily varied to give a good fit to the data: the values of $\beta'(=\beta)$ and r/r'.

Figure 9 shows some more of Chen's experimental results on potassium. It shows the effect of boiling pressure on the IBS for an MBS temperature and pressure of 1166°F and 12·0 psia, respectively. Curve A represents equations (7) and (10), while curve B represents equations (12) and (13). The slightly better fit of curve A is due to the fact that r/r' was set at the particular value of 0·74. As we can see from Figs. 3 and 4.

in the lower range of p'_L, β has relatively little effect on $(t_w - t_{sat})$. Thus, curve A (and presumably curve B also) in Fig. 9 is not sensitive to β or β'. The present author therefore simply chose β' equal to 3×10^{-15}, approximately the same as that in Fig. 8, and assumed β was equal to β' at all values of p_L. It is therefore apparent that, at low values of p'_L, the superheat curve is affected primarily by r/r', and not by β.

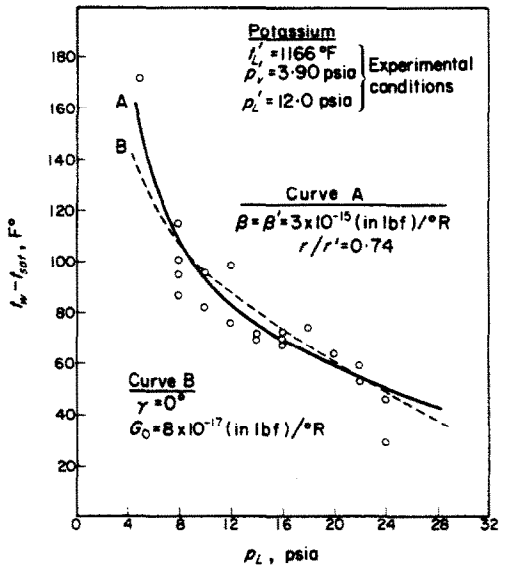

FIG. 9. Effect of boiling pressure on incipient-boiling wall superheats for potassium. Comparison between Chen's experimental results and theoretical curve A based upon equations (7) and (10) and theoretical curve B based upon equations (12) and (13).

Figure 10 presents some further experimental results obtained by Chen [5] showing the effect of variation in t'_L on the incipient-boiling superheats. Here again, the experimental points are well represented by curve B which is the one calculated from equations (7) and (10). Since the MBS pressure was low, the curve is not very sensitive to β. It is based on $\beta' = 3 \times 10^{-15}$, $\beta = \beta'$, and $r/r' = 0·72$.

From the foregoing discussion, it is quite apparent that Chen's [5] experimental results on potassium are well correlated by equations (7) and (10), on the basis of $\beta' = 3 \times 10^{-15}$, $2 \times 10^{-15} \leqslant \beta \leqslant 3 \times 10^{-15}$, and $0·70 \leqslant r/r' \leqslant 0·74$.

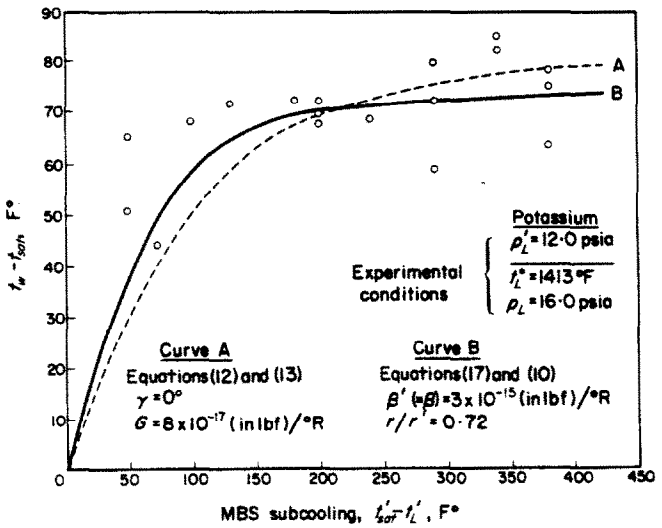

FIG. 10. Comparison between Chen's [5] experimental results and two theoretical curves. Curve A is based upon equations (12) and (13), while curve B is based upon equations (7) and (10).

Sodium

The only incipient-boiling wall superheat results reported in the literature for sodium, where all the relevant variables were controlled and measured, are those recently reported by Holtz and Singer [8]. They measured superheats in pool boiling of sodium in a vertical cylindrical vessel whose i.d. was 1·610 in. and whose heated length was 6·25 in. It was made of type 304 stainless steel, and the inside surface was polished to an average roughness of 8 μin. The vessel was heated with tightly wrapped electrical-resistance heater wire, and the inside wall temperature was determined from the readings of thermocouples inserted in the wall.

Prior to filling with sodium, the entire apparatus was evacuated to a pressure of 2×10^{-6} mm Hg, and the system was then held at a predetermined temperature and pressure for some period of time to effect the MBS condition.

The length of time, however, was not given in the reference. The MBS pressure, p'_L, was increased with each successive MBS treatment. The heat fluxes were low—in the 8700–18,000 Btu/hft^2 range.

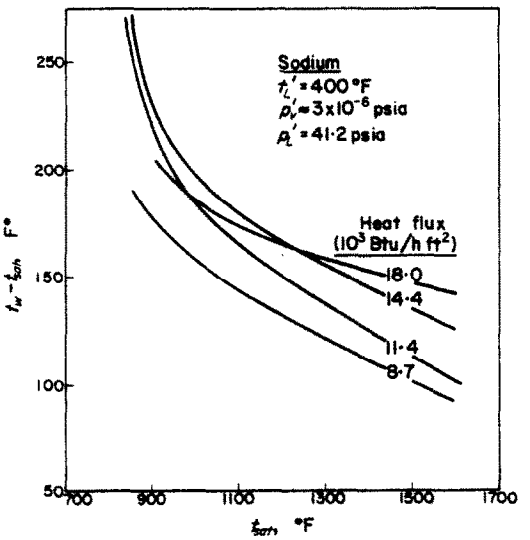

FIG. 11. Incipient-boiling superheat results reported by Holtz and Singer [8] for pool boiling of sodium.

Figure 11 is a reproduction of Fig. 11 in Holtz and Singer's paper. It gives the results of their measurements, showing the effect of saturation temperature (or boiling pressure, p_L) on the incipient-boiling superheat. The MBS conditions were 400°F and 41·2 psia. Presumably, a single MBS step was followed by four series of incipient boiling events, the first series being carried out at a heat flux of 8·7 Btu/(hft^2), and the succeeding ones at fluxes of 11·4, 14·4, and 18·0, in that order. These are actually very low heat fluxes compared with those in a reactor core, for example; but heat flux *per se* is not believed to affect the incipient-boiling wall superheat. It will be noticed that the four curves in the figure have the same general shape as curve A in Fig. 9.

It should be pointed out that the data points which gave the curves in Fig. 11 had considerable spread, averaging roughly ±25 F° for two of the curves and ±50 for the other two. Thus, the data points for the four curves had extremely large overlaps.

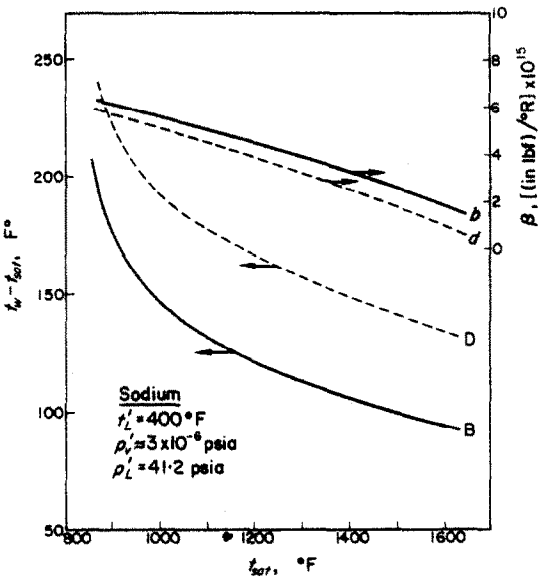

FIG. 12. Theoretical prediction of incipient-boiling wall superheats for sodium, based upon equations (7) and (10). The superheat curves B and D are based upon the β curves *b* and *d*, respectively. The calculated values of r' were 7·43 × 10^{-5} in. and 7·30 × 10^{-5} in. for curves B and D, respectively, and r was assumed equal to r'.

Figure 12 shows two calculated superheat curves which roughly bracket those in Fig. 11. They are based on the same MBS conditions as the experimental curves. Curve B represents a β' value of 6 × 10^{-15} (in. lbf)/°R, with β values as given by curve *b*. It will be noticed that it was assumed that there was no loss of inert gas between the time of the MBS condition and the first incipient-boiling event which was presumed to have occurred at the low end of the t_{sat} scale. It will be further noticed that the rate of loss of inert gas, as indicated by the slope of curve *b*, is actually not very great, when it is realized that a large number of incipient boiling events had occurred in covering the t_{sat} range. This therefore justifies the above assumption. The apparent low rate of inert gas escape from the cavities is consistent with its very low

solubility in liquid metals. For example, the present author estimated an atom fraction of only $1{\cdot}86 \times 10^{-8}$ for the solubility of argon in sodium at 1000°F and 1 atm, from the recent solubility results reported by Veleckis *et al.* [9].

The calculated value of r' for curve B was $7{\cdot}43 \times 10^{-5}$ in., and r/r' was assumed equal to unity. There was no way of determining the true value of this ratio, because there was no experimental curve similar to that in Fig. 8 for potassium, i.e. $(t_w - t_{sat})$ vs. p'_L. One needs to have such a plot, covering a relatively wide range of p'_L. As explained earlier, data at low values of p'_L are more important in determining r/r' than those at high values. In carrying out the calculations reported here, the vapor pressure and surface tension of sodium were taken from Ditchburn and Gilmour [10] and Golden and Tokar [11], respectively.

Superheat curve D in Fig. 12 was obtained by taking β' equal to $5{\cdot}5 \times 10^{-15}$, and then using curve *d* to evaluate β. The calculated value of r' was $7{\cdot}30 \times 10^{-5}$ in. It is seen that a big change in the position of the superheat curve was brought about by only a slight change in the inert gas content. We can therefore conclude that the spread in the curves in Fig. 11 might well have been due to varying amounts of inert gas in the active cavities rather than variation in heat flux. In progressing from the lower to the higher heat fluxes, it is logical that there should have been inert gas losses from the cavities, because of the many incipient-boiling events that had taken place.

As mentioned above, there were insufficient data taken in the study reported by Holtz and Singer to evaluate the ratio r/r'. Therefore, both incipient-boiling superheat curves in Fig. 12 were based on the simple assumption that r/r' equalled unity. To see what the difference would be when r/r' was something less than unity, the curves in Fig. 13 were calculated. The superheat curve in this figure is the same as curve B in Fig. 12. It will be noticed that, in this case, the β curve is higher and has a steeper slope.

It is thus apparent that there is an infinite

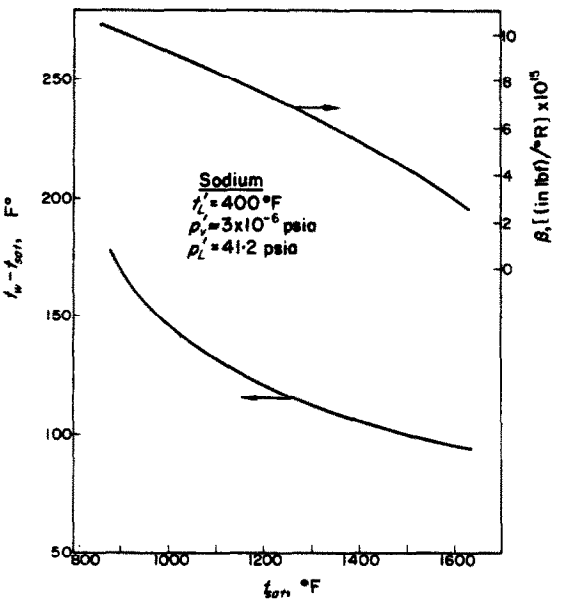

FIG. 13. Theoretical prediction of incipient-boiling wall superheats for sodium, based upon equations (7) and (10). The curve is based upon $\beta' \times 10^{-14}$, $r/r' = 0{\cdot}75$, and the gradual decrease in β as given by the β curve. The value of r' was calculated to be $8{\cdot}2 \times 10^{-5}$ in.

number of combinations of β', β curve, and r/r' which will give the same superheat curve for the MBS conditions of 41·2 psia and 400°F. But, if data had been taken over a range of p'_L rather than at a single value, then there would be only one combination of these parameters that would allow equations (7) and (10) to correlate the results, as we saw in Fig. 8.

It may be wondered why the inert gas content made such a big difference in Fig. 12 but a negligible difference in Fig. 9. The answer is that in Fig. 9, p_G was negligible compared with p_v, whereas in Fig. 12, the reverse is true. This is seen by comparing the p_G values in Tables 1 and 2.

It may also be noticed that the β' values for both the potassium results and the sodium results were found to be of the same order of magnitude, even though the filling pressures were widely different in the two sets of experiments. However, Holtz and Singer's experimental superheat

results were actually very much lower than those predicted by equation (3), indicating the probable presence of considerable inert gas.

EFFECT OF VELOCITY

From what has been said so far, it might be inferred that flow rate would have little effect on the IB wall superheat. But actually, on the basis of limited experimental data, the effect appears to be considerable. For example, Logan, Landoni, and Baroczy [12] observed that the IB bulk superheat decreased from ≈50 to 0°F for sodium flowing vertically upward in a stainless-steel annular test section, as the linear velocity was increased from 2·0 to 4·5 ft/s. The bulk superheat would, of course, be significantly less than the wall superheat. Pinchera *et al.* [13] recently reported similar results for forced-convection flow of sodium past a heated stainless-steel-clad vertical rod.

The mechanism by which flow rate affects IB superheats is not clear, since the locale of the MBS–IB phenomena, according to Holtz, is located inside the cavities or, at worst, at the inner boundary of the so-called laminar layer—well isolated from the turbulent core of the flowing stream. However, it is now well known that eddies do exist right up to the wall, that rapid local temperature fluctuations of the heating surface do occur, and that pressure fluctuations are transmitted to the wall. Thus, time-average values of t_L and p_L—the types we have been considering in equations (9) and (10)—may not be relevant under turbulent-flow conditions. This probably explains why superheats measured under forced-flow conditions generally vary from measurement to measurement considerably more than those measured under nonflow conditions.

There is another possible contributory reason

Table 2. Summary of both MBS *and* IB *conditions pertaining to curves* B *and* D *in Fig.* 12

t_L^* (=t_{sat})	900°F	1100°F	1300°F	1500°F
p'_L [psia]	41·2	41·2	41·2	41·2
p'_v [psia]	neg'l	neg'l	neg'l	neg'l
t'_L [°F]	400	400	400	400
Curve B				
β' [(in. lbf)/°R]	$6{\cdot}00 \times 10^{-15}$	$6{\cdot}00 \times 10^{-15}$	$6{\cdot}00 \times 10^{-15}$	$6{\cdot}00 \times 10^{-15}$
p'_G [psia]	12·58	12·58	12·58	12·58
r' (=r) [in.]	$7{\cdot}43 \times 10^{-5}$	$7{\cdot}43 \times 10^{-5}$	$7{\cdot}43 \times 10^{-5}$	$7{\cdot}43 \times 10^{-5}$
β [(in. lbf)/°R]	$6{\cdot}00 \times 10^{-15}$	$4{\cdot}97 \times 10^{-15}$	$3{\cdot}87 \times 10^{-15}$	$2{\cdot}51 \times 10^{-15}$
p_v [psia]	0·34	1·35	4·50	13·45
p_G [psia]	22·5	20·56	17·65	12·62
p_L [psia]	0·052	0·42	2·15	7·70
t_L (=t_w) [°F]	1075	1235	1410	1600
($t_w - t_{sat}$) [F°]	175	135	110	100
Curve D				
β' [(in. lbf)/°R]	$5{\cdot}50 \times 10^{-15}$	$5{\cdot}50 \times 10^{-15}$	$5{\cdot}50 \times 10^{-15}$	$5{\cdot}50 \times 10^{-15}$
f'_G [psia]	12·13	12·13	12·13	12·13
r' (=r) [in.]	$7{\cdot}30 \times 10^{-5}$	$7{\cdot}30 \times 10^{-5}$	$7{\cdot}30 \times 10^{-5}$	$7{\cdot}30 \times 10^{-5}$
β, [(in. lbf.)/°R]	$5{\cdot}50 \times 10^{-15}$	$4{\cdot}48 \times 10^{-15}$	$3{\cdot}23 \times 10^{-15}$	$1{\cdot}75 \times 10^{-15}$
p_v [psia]	0·51	1·87	6·15	16·60
p_G [psia]	22·30	19·97	15·90	9·41
p_L [psia]	0·052	0·42	2·15	7·70
t_L (=t_w) [°F]	1122	1280	1460	1640
($t_w - t_{sat}$) [F°]	222	180	160	140

why IB superheats are found to decrease sharply as the flow rate is increased: high stream velocities can, in certain situations, result in seal gas entrainment, which in the limit could conceivably reduce the IB superheat to zero.

Much additional work is required before the effect of flow rate on IB superheats is understood. On the basis of present information, however, it appears that under normal flow conditions, IB wall superheats would be negligibly small in a sodium-cooled-reactor core; but in the event of a loss-of-flow incident, it is the no-flow or very-low-flow situation that is relevant.

In the two sets of experimental results discussed in this paper, velocity effects were not of great consequence. Holtz and Singer's data were taken under pool-boiling conditions, and Chen's data were taken at a linear velocity of only 0·2 ft/s, which corresponded to a Reynolds number of 3200. This is barely turbulent flow, which means that the results should not be greatly different from those for either stagnant or natural-circulation conditions.

CONCLUSIONS

1. Incipient-boiling wall-superheat data for liquid metals can be well correlated by equations (7) and (10) if the correct values of β', β, and r/r' are used. The correct values can be determined from the data if they were obtained over a sufficiently wide range of p'_L or t'_L. Under such conditions, there is only one combination of these parameters that allows the equations to correlate a given set of data.
2. The loss of inert gas from an active cavity between the time of the maximum boiling suppression and the time of the first incipient-boiling event appears to be negligibly small. However, for a large number of IB events following a single MBS condition, it is possible to lose the majority of the inert gas from an active cavity.
3. On the basis of the limited data examined in this study, it appears that the most stable radius of curvature of the liquid–vapor interface, r, during superheat conditions (or, in other words, that at the time of nucleation) is smaller than the radius of curvature of the interface, r', at the time of maximum boiling suppression. The data indicated that r was about $\frac{3}{4}$ of r'.
4. It was found in the present study that the value of r' (and also r) was of the same order of magnitude for both Chen's potassium results and Holtz and Singer's sodium results, even though the heating surface was presumably much smoother in the latter situation. This corroborates Holtz's [4] original hypothesis that the size of an active cavity is determined primarily by the MBS conditions and not by the surface roughness.
5. The apparent effect of heat flux on the incipient-boiling wall superheat could be explained, in part, at least, in terms of inert-gas loss from the active cavities, rather than an inherent effect of heat flux itself.

ACKNOWLEDGEMENT

The author is grateful to his colleague, Dr. John C. Chen, for his helpful comments on the original draft of this paper.

REFERENCES

1. V. I. Subbotin, P. A. Ushakov, P. L. Kirillov *et al.*, Heat removal from reactor fuel elements cooled by liquid metals (in Russian), In *Proc. 3rd Int. Conf. on the Peaceful Uses of Atomic Energy, Geneva, Sept.* 1964, Vol. 8, pp. 192–200, United Nations, New York (1965).
2. J. A. Edwards and H. W. Hoffman, Superheat with boiling alkali metals. U.S.A.E.C. Report ANL-7100. *Proc. Conf. Application of High-Temperature Instrumentation to Liquid–Metal Experiments. Argonne National Laboratory, Sept.* 28–29, pp. 515–534, 1965.
3. K. H. Spiller, G. Grass and D. Perschke, Superheating and single bubble ejection with the vaporization of stagnate liquid metals, *Atomkernenergie* 12, 111–114 (1967).
4. R. E. Holtz, The effect of the pressure-temperature history upon incipient-boiling superheats in liquid metals, U.S.A.E.C. Report ANL-7184, Argonne National Laboratory, Argonne, Illinois, June 1966.

5. J. C. CHEN, Incipient boiling superheats in liquid metals, *Trans. Am. Soc. Mech. Engrs, J. Heat Transfer C*, **90**, 303–312 (1968).
6. W. T. HICKS, Evaluation of vapor-pressure data for mercury, lithium, sodium, and potassium, *J. Chem. Phys.* **38**, 1873–1880 (1963).
7. J. W. COOKE, Surface tension of potassium. In *Studies in Heat Transfer and Fluid Mechanics*, Progr. Report, 1 October, 1963 to 30 June 1964, H. W. HOFFMAN and J. J. KEYES, U.S.A.E.C. Report ORNL-TM-1148, Oak Ridge National Laboratory (1965).
8. R. E. HOLTZ and R. M. SINGER, On the initiation of pool boiling in sodium, Paper presented at the *Tenth National Heat Transfer Conference*, Philadelphia, Pa., 11–14 August (1968).
9. E. VELECKIS, R. BLOMQUIST, R. YONCO and M. PERIN, Solubility of argon in liquid metals, U.S.A.E.C. Report ANL-7325, *Argonne National Laboratory, Argonne, Illinois, Chemical Engineering Division Semi-annual Report, July–December*, pp. 128–131 (1966).
10. R. W. DITCHBURN and J. C. GILMOUR, The vapor pressures of monatomic vapors, *Rev. Mod. Phys.* **13**, 310–327 (1941).
11. G. H. GOLDEN and J. V. TOKAR, Thermophysical properties of sodium. U.S.A.E.C. Report ANL-7323, Argonne National Laboratory, August, p. 61 (1967).
12. D. LOGAN, J. LANDONI and C. BAROCZY, Nuclear safety (kinetics)—boiling studies, U.S.A.E.C. Report NAA-SR-12492, Atomics International, pp. 121–126 (1967).
13. G. C. PINCHERA, G. TOMASSETTI, L. FALZETTI and G. FORNARI, Sodium boiling research related to fast reactor safety. *Trans. Am. Nucl. Soc.* **11**, 691–692 (1968).

SURCHAUFFES PARIÉTALES AU DÉBIT DE L'ÉBULLITION DANS LES MÉTAUSE LIQUIDES

Résumé—On motre qu'un bon accord entre les surchauffes pariétales au début de l'ébullition prévues et mesurées peuvent être obtenues avec le modèle original de surchauffe de Holtz [4], si deux facteurs additionnels sont pris en considération. Le premier de ceux-ci est la perte de gaz inerte de la cavité entre le temps de la suppression maximale de l'ébullition (MBS) et le temps du début de l'ébullition (IB). Le second de ceux-ci est la probabilité que le rayon de courbure de l'interface liquide–vapeur à IB puisse être sensiblement différent de celui à MBS.

En se basant sur les résultats expérimentaux récents d'IB obtenus par Chen [5] sur le potassium et ceux obtenus par Holtz et Singer [8] sur le sodium, on a essayé de tirer les conclusions suivantes:

(a) la perte de gaz inerte à partir d'une cavite active entre le temps de MBS et celui du premier IB semble être négligeable, mais elle peut être considérable si un grand nombre d'événements IB suivent un seul traitement MBS;

(b) le rayon de la bulle à IB est environ 3/4 de celui à MBS;

(c) le fini de la surface pour des surfaces lisses moyennes ne semblerait pas avoir une forte influence sur les surchauffes IB;

(d) l'effet apparent de flux de chaleur pourrait être en réalité un effet de gaz inerte.

Zusammenfassung—Es wird gezeigt, dass eine gute Übereinstimmung der berechneten und gemessenen Wandüberhitzungen bei plötzlichem Sieden erzielt werden kann, wenn bei dem urparünglichen Modell der Überhitzung von Holtz [4] zwei zusätzliche Faktoren berücksichtigt werden. Der erste Faktor ist der Verlust an Inertgas zwischen dem Zeitpunkt des maximalen Siedeverzugs (MBS) und dem Augenblick des plötzlichen Siedens (IB). Der zweite Faktor ist die Wahrscheinlichkeit, dass der Krümmungsradius der Dampf–Flüssigkeitsgrenzfläche bei IB wesentlich verschieden ist von dem Krümmungsradius bei MBS.

Auf Grund neuerer Untersuchungsergebnisse bei IB von Chen [5] mit Kalium und von Holtz und Singer [8] mit Natrium wurden folgende Schlüsse versuchsweise gezogen:

(a) Der Verlust an Inertgas eines aktiven Keims in der Zeit zwischen MBS und dem ersten IB scheint vernachlässigbar klein zu sein; er kann aber beträchtlich werden, wenn häufige IB-Zustände einem einzelnen MBS-Zustand folgen; (b) Der Blasenradius bei IB ist etwa $\frac{3}{4}$ dem bei MBS; (c) Oberflächenbehandlung bei normal glatten Oberflächen scheinen keinen grossen Einfluss auf die IB-Überhitzung zu haben; (d) Der augenscheinliche Einfluss des Wärmestrons kann möglicherweise in Wirklichkeit ein Einfluss des Inertgases sein.

Аннотация—Показано, что с помощью оригинальной модели перегрева Холца (4) можно получить хорошее соответствие между расчетными и измеренными перегревами стенки при начале кипения с учетом двух дополнительных факторов. Первым фактором является потеря инертного газа из полости в период между максимальным подавлением кипения и началом кипения. Вторым фактором является вероятность того, что радиус

кривизны поверхности раздела жидкость-пар при начале кипения может значительно отличаться от радиуса при максимальном подавлении кипения.

На основе недавних результатов при начале кипения, полученных Ченом (5) для калия, и результатов Холца и Сингера (8) для натрия можно сделать следующие выводы: (*а*) оказывается, что потеря инертного газа из активной полости в период между максимальным подавлением кипения и началом кипения пренебрежимо мала, но она может быть значительна, если несколько случаев начинающегося кипения следует за одним случаем максимального подавления кипения; (*б*) радиус пузырька при начале кипения составляет $\frac{1}{2}$ радиуса для случая максимального подавления кипения; (*в*) оказывается, что обработка поверхности для обычных гладких поверхностей не влияет сильно на перегрев при начале кипения; (*г*) кажущееся влияние теплового потока в действительности может быть влиянием инертного газа.